Wear Behaviour of a Plasma-Sprayed Al_2O_3-13%TiO_2 Ceramic Coating/Steel Couple Under High Constant and Variable Loads

C. Soffritti, R. Vazquez Aguilar, A. Fortini, M. Merlin, G.L. Garagnani

This work investigates the effects of heavy loadings on an Al_2O_3-13%TiO_2 ceramic coating/steel couple under dry sliding and in conditions similar to those occurring in heavy-duty diesel engines. Two types of wear tests were performed by a standard pin-on-disc tribometer under high constant and variable loads. Before wear tests, microstructure and mechanical properties of coating and steel were determined by optical emission spectrometry, optical microscopy, roughness, hardness, fracture toughness, elastic modulus and X-ray diffractometry. The coefficient of friction was instantly calculated by the tribometer. The wear rate of Al_2O_3-13%TiO_2 ceramic coating was evaluated by the wear volume and that of pins by weighing them before and after the tests. The wear depth of pins was calculated by measuring the decrease in length by calipers before and after the tests. The wear tracks on pins and coating surfaces were analyzed by X-ray diffractometry and by scanning electron microscopy with energy-dispersive spectroscopy. For all loads except the lowest constant one, the results indicated high friction and wear involving material removal from the coating surface, through a severe-oxidational wear associated with extensive cracking of the surface of the coating, softening of the carburizing steel and removal of the carburized layer of pins. The wear mechanism was between mild- and severe-oxidational under the lowest constant load, which was therefore suggested as the limit for acceptable performance of the sliding couple under study.

KEYWORDS: DIESEL ENGINES – HEAVY LOADINGS – CARBURIZING STEEL – PLASMA-SPRAYED COATINGS – WEAR

INTRODUCTION

Friction and wear are the major causes of loss of mechanical performances and energy dissipation in engine subsystems such as the engine block with pistons and cylinders, the transmission, the fuel system, the valve train and the exhaust system [1]. Concerning wear resistance of mechanical components, thermal-sprayed ceramic coatings on steel represent an efficient and economical alternative, when common thermo-mechanical processes and heat treatments are inadequate. These coatings may exhibit high hardness and chemical stability, are able to withstand high temperatures and are resistant to many corrosive environments. Some types of ceramics have already found application in engineering as tribological components, for example in cylinder head fire decks, piston crowns, exhaust valve faces and braking devices [2,3]. Among thermal-sprayed ceramic coatings, plasma-sprayed of Al_2O_3-TiO_2 coatings provide protection against abrasive wear superior to that of traditional wear resistant hard chromium [4,5] and molybdenum [6,7] coatings. Under dry sliding conditions, plasma-sprayed Al_2O_3-TiO_2 coatings are known to form a porous tribofilm composed of plastically deformed wear debris, which does not protect the substrate from wear [4]. On these ceramic coatings, many different wear mechanisms are detected, involving abrasive wear [8], delamination and crack nucleation [9,10], and adhesive wear [9]. Several studies deal with the sliding wear resistance

C. Soffritti, A. Fortini, M. Merlin, G.L. Garagnani
Department of Engineering (DE), University of Ferrara,
via Saragat 1, 44122 Ferrara, Italy

R. Vazquez Aguilar
Facultad de Arquitectura,
Universidad Autonóma de Coahuila, Blvd. Los Fundadores,
Ciudad Universitaria,
CP 25350, Arteaga,
Coahulla, Mexico

of ceramics against steel [4,11–19]. In [4], the wear resistance of a plasma-sprayed Al_2O_3-13%TiO_2 coating/steel couple has been investigated through pin-on-disc testing, and correlated to microstructural and micromechanical characteristics: the results showed that the ceramic coating exhibits high friction and wear, and inflicts high wear on the counterpart.
In common operating conditions, most components under mechanical loading undergo dynamic rather than static stresses. Recently, the effects of variable loads on wear resistance of carbon steel in unlubricated condition have been extensively investigated [20,21]. A "quasi-mild wear mode" has been proposed, resulting from the generation of a severely oxidized, work-hardened surface under heavier loads. Its appearance is apparently affected by several factors such as the sliding distance at low loads before an increase in load, the morphology of wear debris, the flattening and degree of oxidation of the worn surfaces [22,23].
The effects of heavy loading and sliding speed conditions have been previously evaluated for a plasma-sprayed Al_2O_3 coating in dry sliding conditions, using a pin-on-disc tribometer [24]. Our study investigates the tribological effects of high constant and variable loads on a plasma-sprayed Al_2O_3-13%TiO_2 ceramic coating in dry sliding contact with carburizing steel, in conditions similar to those occurring in heavy-duty diesel engines. Two types of wear tests were conducted, respectively, under high constant and variable loads using a standard pin-on-disc tribometer.

EXPERIMENTAL PROCEDURE

Substrate and coating

In this study, a carburized steel disc (80 mm in diameter, 6 mm in thickness) was used as a substrate in the deposition of a 190 µm-thick ceramic coating of Al_2O_3-13%TiO2. To improve ceramic adhesion, a 20 µm-thick Ni-20%Cr bond coat was deposited directly onto the steel substrate. Both top and bond coatings were obtained by air plasma spray (APS) technique. The chemical composition (wt. %) of discs and pins used for wear tests was determined by a SPECTROLAB OES analyzer (SPECTRO Analytical Instruments GmbH, Kleve, Germany) and is listed in Tab.1 The feedstock powders characteristics and chemical composition of top and bond coatings, provided by the manufacturer, are summarized in Tab.2 The plasma spray operating parameters were confidential.

Tab. 1 – Chemical composition (wt. %) of discs and pins used for wear tests.

Chemical composition (wt. %)											
	C	**Mn**	**Ni**	**Cr**	**Si**	**Cu**	**Mo**	**S**	**V**	**P**	**Fe**
Disc	0.22	0.88	0.87	0.84	0.30	0.20	0.06	0.03	0.02	0.02	Bal.
Pin	0.23	0.86	0.95	0.91	0.26	0.10	0.06	0.02	0.02	0.01	Bal.

Tab. 2 – Feedstock powder characteristics and chemical composition of top and bond coatings.

	Al_2O_3-13%TiO_2	Ni-20%Cr
Feedstock powder type	FST C-335.23	Metco 43CNS
Chemical composition [wt. %]	13.12 % TiO2, 0.22 % ZrO2, 0.1 % SiO2, 0.09 % MgO, 0.07 % CaO, 0.39 % other oxides, balance Al_2O_3	19.07 % Cr, 1.1 % Si, 0.4 % Fe, 0.02 % C, balance Ni
Particle dimensions [µm]	-45 + 15	-45 + 15

The coating microstructure was investigated by X-ray diffractometry (XRD) with a Philips X'PERT PW3050 diffractometer (Philips, Amsterdam, Netherlands), using Cu K-alpha radiation (λ = 1.54 Å), with an intensity scanner versus diffraction angle between 15° and 120° (0.06° step size, 2 s/step scanner velocity and 1.5 grid), a 40 kV voltage and a 30 mA filament current. Properly polished cross-sections were also examined by a Zeiss EVO MA 15 (Zeiss, Oberkochen, Germany) scanning electron microscope equipped with an Oxford X-Max 50 (Oxford Instruments, Abingdon-on-Thames, UK) microprobe for energy-dispersive spectroscopy (SEM/EDS) and a Leica MEF4 M (Leica, Wetzlar, Germany) optical microscope. The SEM micrographs were recorded in secondary electron imaging (SEI-SEM) and back-scattered electron (BSE-SEM) mode. The optical micrographs were processed by an image analysis software to evaluate coating porosity. Roughness parameters (Ra and Rz) were calculated by a Talysurf CCI-Lite non-contact 3D profilometer (Taylor-Hobson, Leicester, UK). Before each measurement, all coating surfaces were cleaned in an ultrasonic bath. Hardness (300 gf load and 15 s loading time) and fracture toughness (1000 gf load) were measured on polished cross-sections of the coating by a Future-Tech FM-110 Vickers microindenter

(Future-Tech Corp., Kawasaki, Japan). A mean of 15 indentations were carried out for each hardness and toughness measurement. Fracture toughness was assessed by measuring the length of indentation diagonals and cracks through optical micrographs, employing the Evans–Wilshaw equation:

$$K_{IC} = 0.079 \left(\frac{P}{a^{3/2}}\right) log\left(4.5\frac{a}{c}\right) \quad (1)$$

where a is the half-length of indentation diagonal (μm), c is the crack length (μm) and P is the load (mN). This formula was developed for "half-penny-shaped" cracks, but it is considered valid also for Palmqvist cracks when the ratio between the crack and the half-length of diagonal indentation is between 0.6 and 4.5 [25,26]. A depth-sensing Nanotest 550 microindenter (Micro Materials Ltd., Wrexham, UK) was employed to measure elastic modulus on polished cross-sections of the coating. Elastic modulus was calculated from the unloading part of instrumented indentation loading-unloading curves, by the Oliver–Pharr formula [27]. A 5 N indentation load was chosen, with 5 N/min loading rate, 4 N/min unloading rate, 15 s loading time and a minimum of 15 indentations was performed.

Sliding wear tests

Pin-on-disc dry sliding tests were conducted by using the Multispeciment Tester tribometer, supplied by Ducom Instruments of Bengaluru (India) in accordance with ASTM G99-17 standard. Cylindrical steel pins (6 mm in diameter, 22 mm in height) were used as a counterbody material. All unworn surfaces of original pins were carburized up to about 500 μm in depth.
This value represents the effective thickness, i.e., the thickness of the material layer with hardness equal or greater than 550 kgf/mm^2 [28]. The Vickers hardness (500 gf load and 15 s loading time) was determined on cleaned cross-sections of the pins by the Future-Tech FM-110 microindenter (Future-Tech Corp.). The measurements were taken at a distance of about 100 μm from the sliding interface, up to about 13 mm in depth. Wear tests were performed at room temperature and in dry conditions. Tests were conducted under two different conditions of normal load: (1) under a constant load of 250, 450 and 650 N, at a sliding speed of 1 m/s, for a total sliding distance of 7500 m; (2) under variable load in a range between 250 and 650 N, with an increase of 100 N every 30 min (corresponding to a sliding distance of 1500 m), at a sliding speed of 1 m/s and for a total sliding distance of 7500 m. All measurements were repeated five times for each condition of applied load. The coefficient of friction (COF) was instantly calculated by the tribometer. The total wear of pins and discs was measured by a Gefran PY-2-F-010-S01 M linear voltage resistance transducer (LVRT) (Gefran, Brescia, Italy) (accuracy: 1 μm) and quantified with a potentiometric wear measuring device.

Characterization of the worn surfaces

The wear rate of the coated discs was evaluated by measuring the cross-section area of the wear track with the Talysurf CCI-Lite non-contact 3D profilometer (Taylor-Hobson). Each area value, obtained as an average of five measurements of cross-section areas along the wear track, was used to calculate the wear volume. The wear rate of pins was assessed by weight measurements before and after tests using a microbalance (METTLER TOLEDO, Columbus, Ohio, USA) with a resolution of 0.01 mg. Weight loss was converted into volume loss by dividing it by the material density. The wear depth of pins was calculated by measuring the decrease in length by calipers before and after tests. In order to clarify the wear mechanisms, the worn surfaces of the coating were investigated by XRD with the Philips X'PERT PW3050 diffractometer (Philips). The wear tracks on pins and coating surfaces were then observed by SEM/EDS with the Zeiss EVO MA 15 scanning electron microscope (Zeiss) equipped with the Oxford X-Max 50 microprobe (Oxford Instruments) for semi-quantitative EDS analyses. Finally, the worn cross-sections of pins were characterized by optical microscope analyses with the Leica MEF4 M (Leica) and Vickers hardness measurements at 500 gf load and 15 s loading time by the Future-Tech FM-110 microindenter (Future-Tech Corp.). The Vickers hardness measurements were taken at a distance of about 100 μm from the sliding interface, up to about 20 mm in depth.

RESULTS AND DISCUSSION

Microstructure and mechanical properties

The cross-sectional morphology of the Al_2O_3-13%TiO_2 coating with the elements distribution is shown in Fig. 1. The Al_2O_3-13%TiO_2 exhibits the typical lamellar microstructure of a plasma-sprayed ceramic coating, characterized by partially melted particles and long inter- and intra-lamellar cracks. Isolated light gray Ti-rich splats are also visible, suggesting the inhomogeneous interdissolution of alumina and titania phases during the spraying process [4,29]. The irregular Ni-20%Cr bond coat promotes the adhesion of the ceramic coating to the steel substrate, in spite of the presence of rare pores and sandblast residues. The porosity is about 13 %, as determined by image analysis, due to splat-stacking faults [4]. The XRD diffractograms recorded on the surface of Al_2O_3-13%TiO_2 coating before wear tests revealed the presence of metastable γ-Al_2O_3 (due to splats quenching) and minor quantities of α-Al_2O_3 as crystalline phases, and glassy phase (Fig. 2). The mean value of Vickers hardness measured on the coating cross-section is 7.78

± 0.5 GPa, whereas those of the roughness parameters are 0.25 ± 0.01 μm (Ra) and 2.66 ± 0.24 μm (Rz). The mean fracture toughness of the Al_2O_3-13%TiO2 coating calculated by Eq. (1) is 1.93 ± 0.65 MPa $m^{1/2}$. The mean value of elastic modulus results in 128 ± 9 GPa.

Optical micrographs of the cross-section of the pin before wear tests are reported in Figs. 3a,b. As seen, the carburized layer shows a martensitic microstructure with low carbide content (Fig. 3a), whereas the non-carburized material is characterized by lower bainitic microstructure (Fig. 3b). The Vickers hardness profile resulting from the carburizing treatment is depicted in Fig. 3c. At the surface, the Vickers hardness is maximum and then decreases toward the inside, finally reaching the typical value of the non-carburized steel at the core of the material. The Vickers hardness profile also confirms an effective thickness of about 500 μm for the carburizing treatment.

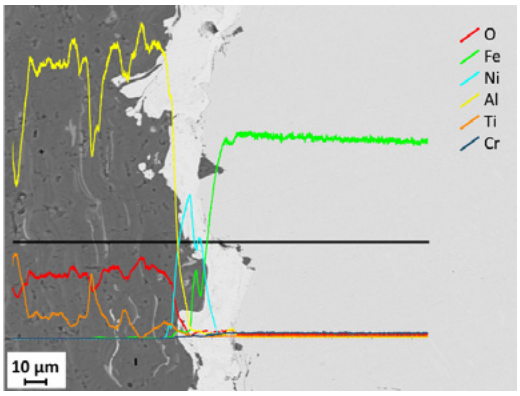

Fig. 1 – BSE-SEM micrograph of the cross-sectional morphology of Al²O³ -13%TiO² coating with the elements distribution.

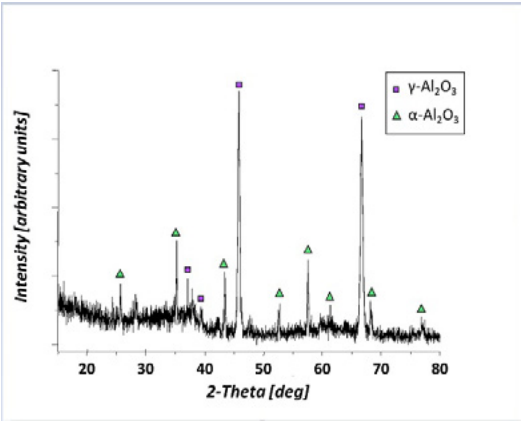

Fig. 2 – XRD diffractogram recorded on the surface of Al²O³ -13%TiO² coating before wear tests.

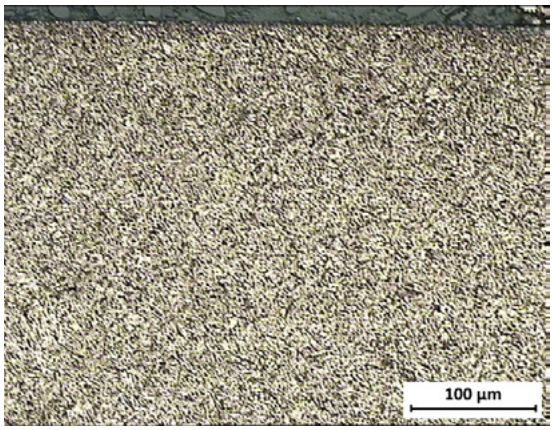

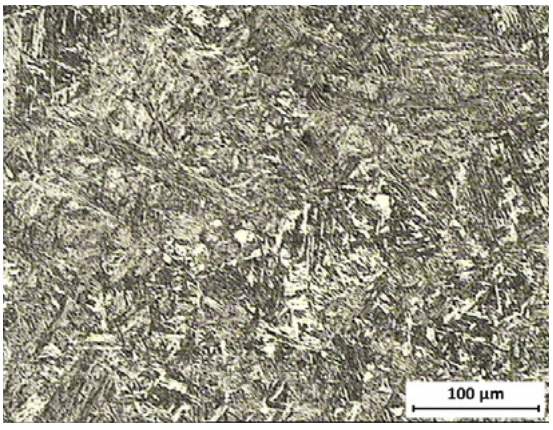

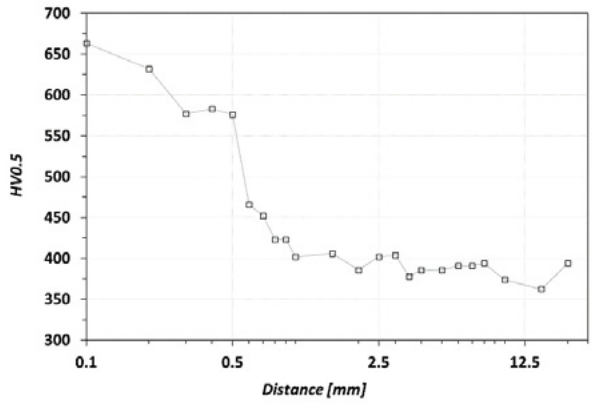

Fig. 3 – (a, b) Optical micrographs of the microstructure of pins in cross-section before wear tests; (c) Vickers hardness profile resulting from the carburizing treatment, measured from 0.1 mm from the sliding interface up to about 13 mm in depth.

Wear tests

The COF and the total wear variations against sliding distance under constant load (250 N, 450 N and 650 N) and under variable load (from 250 N to 650 N) are summarized in Fig. 4. Under a constant 250 N load (Fig. 4a) the COF maintains a quasi-steady state ($\mu \approx 0.10$) until the end of the tests. Under constant loads of 450 N and 650 N (Fig. 4b,c) the COF curves follow a similar pattern. At the beginning of each test, the COF maintains a quasi-steady state ($\mu \approx 0.15$) up to a sliding distance of about 4000 m for 450 N and 2000 m for 650 N, and then rapidly increases up to about 0.35 for 450 N and 0.40 for 650 N. Under variable load (Fig. 4d) a running-in wear takes place until about 1500 m, after which a quasi-steady state ($\mu \approx 0.32$) is reached. Nevertheless, small COF variations occur at sliding distances of about 3000, 4500 and 6000 m, corresponding to the transitions 350/450, 450/550 and 550/650 N in the applied load. In all cases, the increase of COF values may be related to the metal transfer from pins onto Al_2O_3-13%TiO_2 coatings. The mean COF data calculated over the five tests under the higher constant loads and the variable load are similar (between 0.25 and 0.32), but that under the constant load of 250 N is 0.11. The recorded values are slightly lower than previously reported COF values for plasma sprayed Al_2O_3 coating/steel couple under dry sliding and heavy loading conditions [24].

Concerning the total wear variation, under a constant 250 N load the values are negative until the end of tests (Fig. 4a). Under the constant loads of 450 N and 650 N (Fig. 4b,c) the total wear curves follow a similar pattern: the total wear is negative up to a sliding distance of about 7000 m for 450 N and 5500 m for 650 N, and then it progressively increases, reaching final positive values of about 0.06 and 0.29 mm, respectively. Under variable load, the total wear variation is negative until about 2500 m, then slowly increases reaching a final positive value of about 0.92 mm (Fig. 4d). One slope change may also be observed at a sliding distance of about 5000 m, corresponding to the 550/650 N transition in the applied load. In all cases, the negative total wear suggests pin lifting due to material build-up at the Al_2O_3-13%TiO2 coating/steel pins interface. As reported in [17,30], the tribofilm is generated by wear particles sufficiently small to penetrate the grooves and later be sintered by the high temperature at the surface (e.g. due to high load conditions). As sliding continues, the fragmentation of the tribofilm occurs and the total wear becomes positive: the surface layers of the tribofilm, partially removed, may produce wear debris between the sliding surfaces, acting as three-body abradens [17].

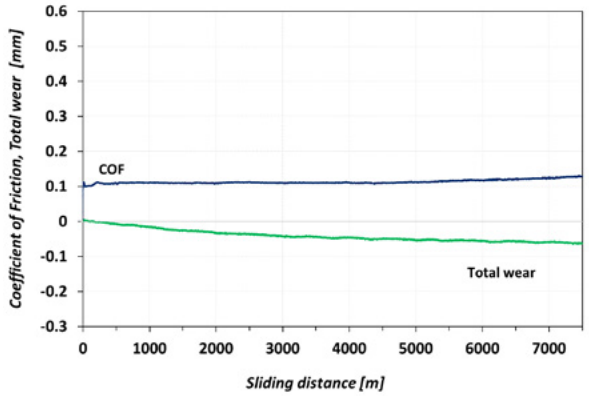

(a)

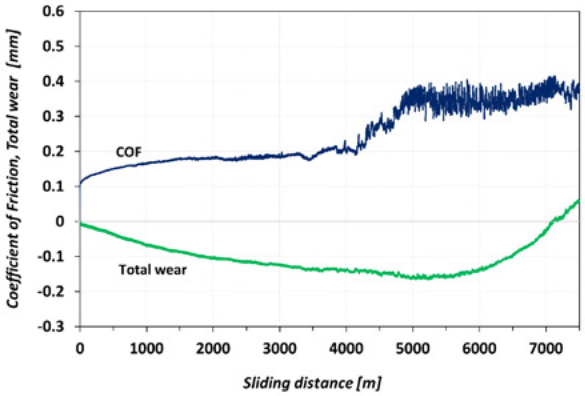

(b)

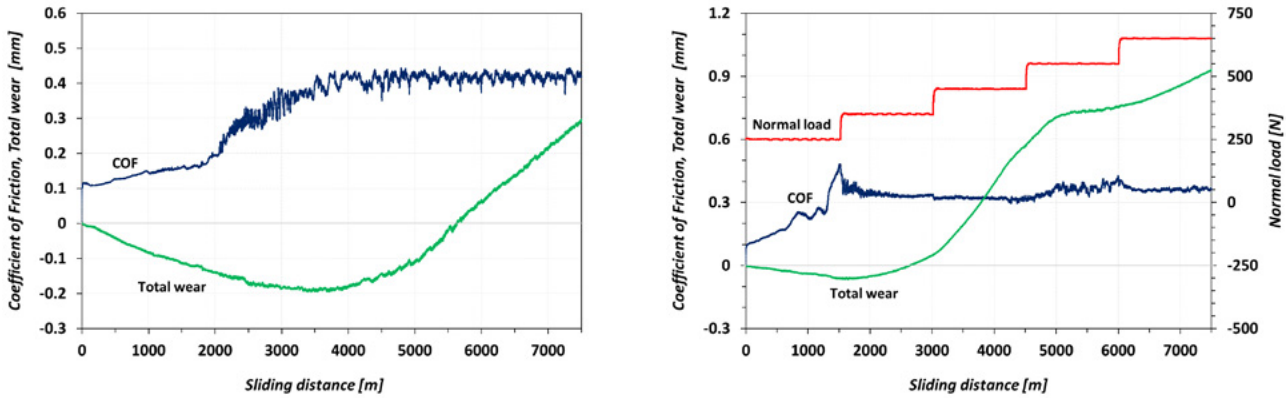

Fig. 4 – Variations of COF and total wear with sliding distance in different conditions: (a) constant 250 N load, (b) constant 450 N load, (c) constant 650 N load and (d) variable 250-650 N load.

The mean wear rates of pins and Al_2O_3-13%TiO_2 coating in all tested conditions are reported in Fig. 5. In any case, the pin undergoes a significant loss of material. Especially, the mean wear rate of pins is in the range of $2 \div 4 * 10^{-6}$ $mm^3/(Nm)$. Studies concerning the wear resistance of carbon steels under dry sliding assess that when the mean wear rate is higher than $1 * 10^{-8}$ $mm^3/(Nm)$, the wear may be considered severe [31,32]. Besides, other authors suggest that higher mean wear rates correspond to higher friction temperatures [31–34]. Concerning the Al_2O_3-13%TiO_2 coating, when the wear tests are performed under constant loads, the mean wear rates increase with increasing load. When the constant 250 N load is applied, the mean wear rate is the lowest. Under variable load, the mean wear rate is comparable to that recorded under the constant 450 N load. Comparing the obtained mean wear rates of the Al_2O_3-13%TiO_2 coating with previous research on wear of sintered ceramics [35,36], the present Al_2O_3-13%TiO_2 coating is under a severe wear regime for all constant loads except at the constant 250 N load where the wear regime is between mild and severe.

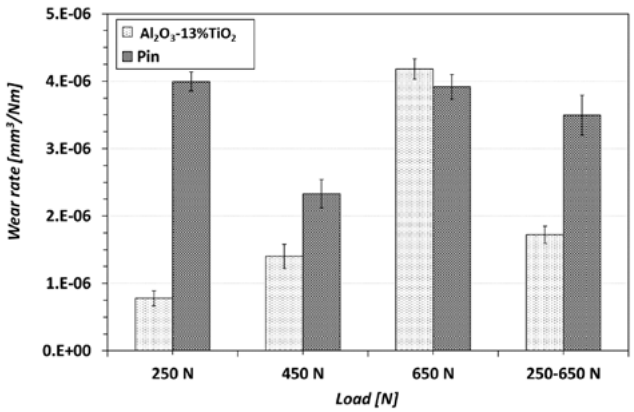

Fig. 5 – Mean wear rates of pins and Al_2O_3-13%TiO_2 coatings in all tested conditions. Error bars represent standard deviation.

Characterization of the worn surfaces: SEM/EDS and optical microscope observations, and XRD analyses

The SEI-SEM micrographs of the worn surfaces of Al_2O_3-13%TiO_2 coating after wear tests under variable load and under the constant 250 N load are shown in Figs. 6a,b and Figs. 6c,d, respectively. Two types of morphologies may be identified on the worn surfaces of Al_2O_3-13%TiO_2 coating after wear tests under variable load: (i) material removal for delamination of the surface layers, with pits and microcracks randomly distributed over the wear track (Fig. 6a), and (ii) metallic film deposition (Fig. 6b). In the first case, during dry sliding, microcracks and dislocation networks may produce wear debris as detected inside pits. The wear particles are entrapped in the contact interface and subjected to continued fracture, deformation or chemical reaction, producing microsized powders [4,37]. In agreement with the literature information, the amount of wear debris

increases with increasing load. Moreover, the pits are deeper in higher loading conditions [4,37]. Regarding to the metallic film deposition, the tribofilm is firmly attached to the Al_2O_3-13%TiO_2 coating because of the strong adhesion between the sliding surfaces: it is plastically deformed and oriented in the direction of the sliding motion. The tribofilm, detected by SEM/EDS, also suggests an oxidational wear mechanism. Previous research stated that, under a mild-oxidational wear regime, oxidation is caused by frictional heating [30]; when a transition to severe-oxidational wear occurs, extended oxidation may be observed and the tribofilm is thicker and more plastic. For the constant loads of 450 and 650 N, the morphology of the worn surfaces of Al_2O_3-13%TiO_2 coating is similar to that under variable load. The amount of metallic film deposition may be compared to the metal transfer observed in Fig. 6b, but the pits are shallow.

Under the constant 250 N load, the amount of metallic film deposition on the worn surfaces of Al_2O_3-13%TiO_2 coating is lower than that observed under the higher constant loads and the variable load (Figs. 6c,d).

Comparing the semi-quantitative EDS analyses of the elements in the tribofilm and in other regions of the wear track, the percentage of iron in the tribofilm is about five times higher than in the rest of the wear track (Fig. 7). The XRD examinations on the tribofilm (Fig. 8) identifies Fe_2O_3, a ferrous oxide that forms when the temperature at the contact surface raises over 200 °C and remains stable when the temperature lowers to room temperature.

The SEI-SEM micrographs of the worn surfaces of pins after wear tests under variable load and under the constant 250 N load are depicted in Fig. 9a and Fig. 9b, respectively. Under variable load (Fig. 9a) and the constant loads of 450 and 650 N, a very rough and plastically deformed metallic film of iron oxide uniformly covers the worn surfaces, with ploughing and cutting appearance. On the contrary, for the constant 250 N, the worn surfaces show a lower amount of metallic oxide (Fig. 9b).

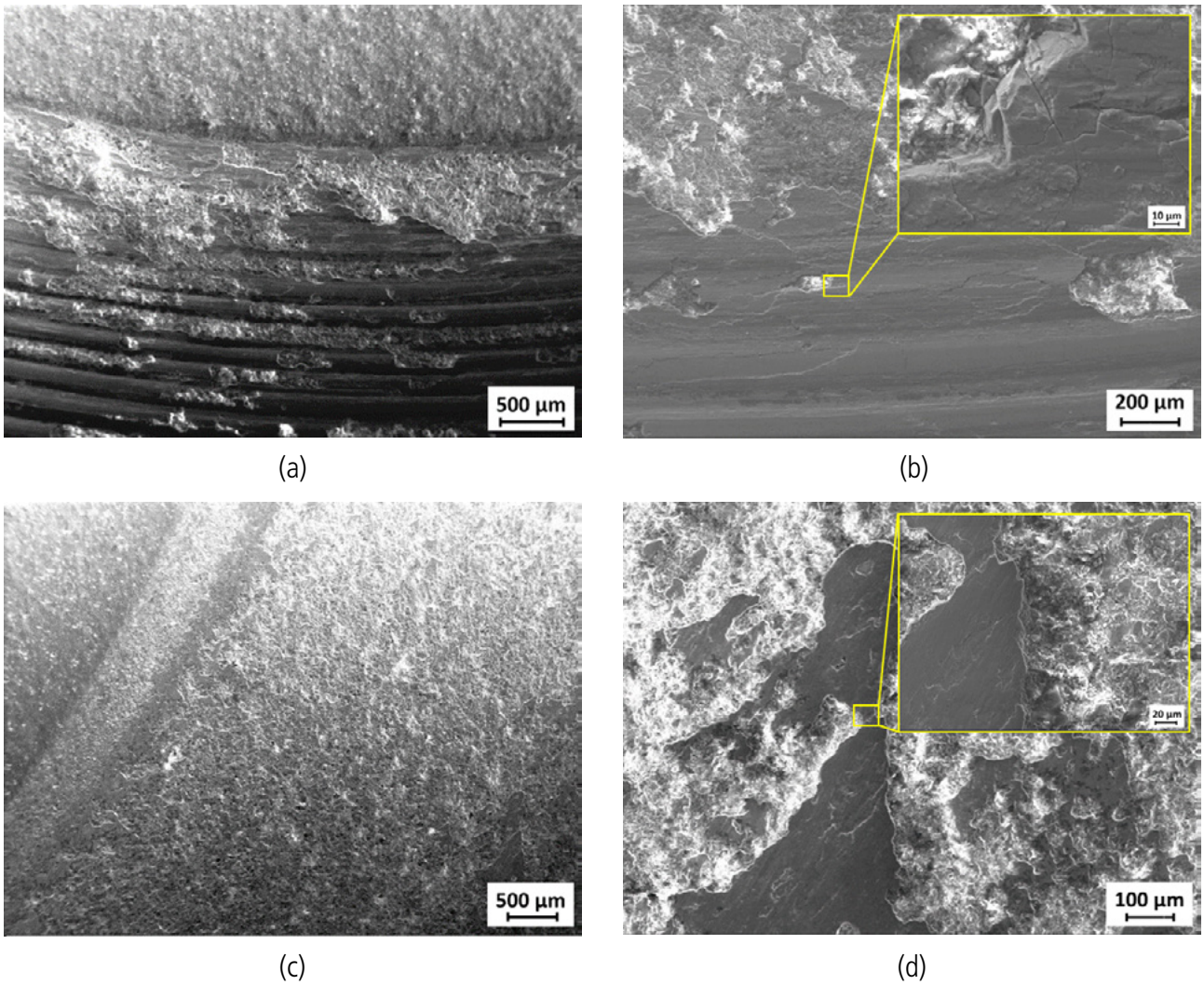

Fig. 6 – SEI-SEM micrographs of the worn surfaces of Al_2O_3-13%TiO_2 coating after wear tests (a, b) under variable load and (c, d) under the constant 250 N load.

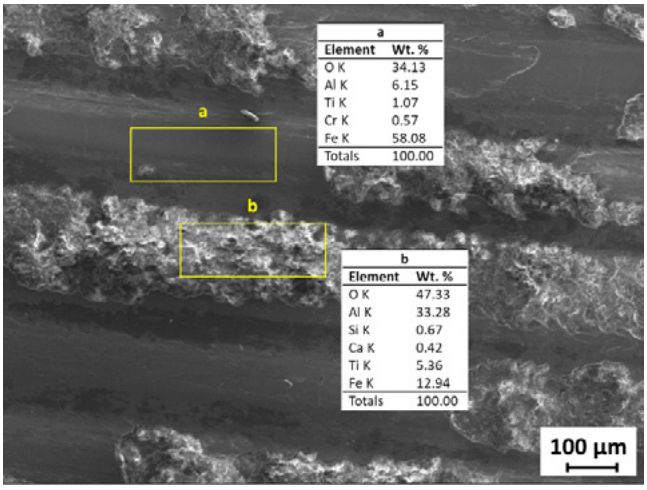

Fig. 7 – SEI-SEM micrograph of Al_2O_3-13%TiO_2 coating after wear tests under variable load, together with the semi-quantitative EDS analyses (wt. %) of (a) the tribofilm and of (b) another region of the wear track.

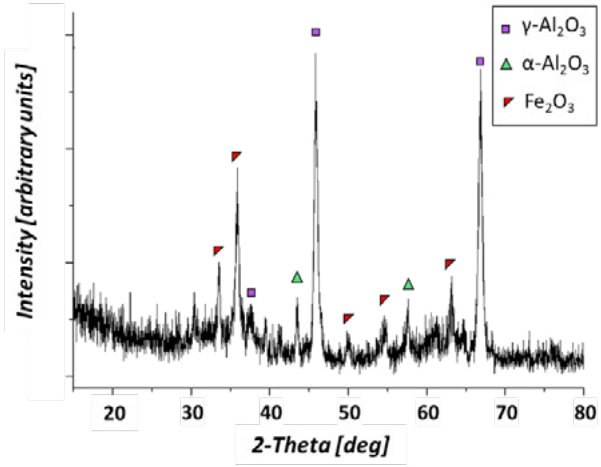

Fig. 8 – XRD diffractogram recorded on the surface of the Al_2O_3-13%TiO_2 coating after wear tests.

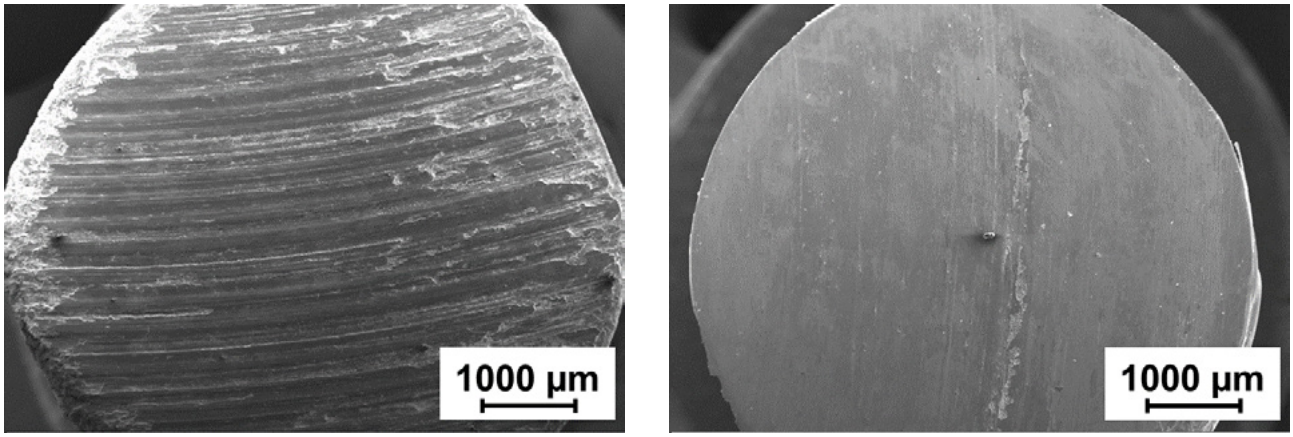

Fig. 9 – SEI-SEM micrographs of the worn surfaces of pins after wear tests (a) under variable load and (b) under the constant 250 N load.

An example of an optical micrograph of the cross-section of pins after wear tests under variable load and the higher constant loads is reported in Fig. 10. Beginning from the worn surface, the sliding wear between Al_2O_3-13%TiO_2 coating and carburizing steel results in a porous and spalled iron oxide layer about 50 µm in thickness (the dark gray layer in Fig. 10). During the tests, it is continuously removed and reformed and does not protect the coating, accounting for the high mean wear rates. The microstructure is then composed of a very fine and unoriented layer, a fine and oriented layer, a plastically deformed layer and the unaffected microstructure. The layered microstructure indicates that severe-oxidational wear involves a series of processes, such as shear fracture and plastic deformation of the surface layers. It is known that the thickness of the plastically deformed layer is related to the properties of the material itself [31,34]. Microstructures with low thermal conductivity, such as the martensitic plus carbide microstructures, are difficult to deform, thus promoting an increase in surface temperature and the formation of a thin plastically deformed layer. For the constant 250 N load, the layers of the microstructure are less evident and the spalled iron oxide is less than 50 µm thick (Fig. 11).

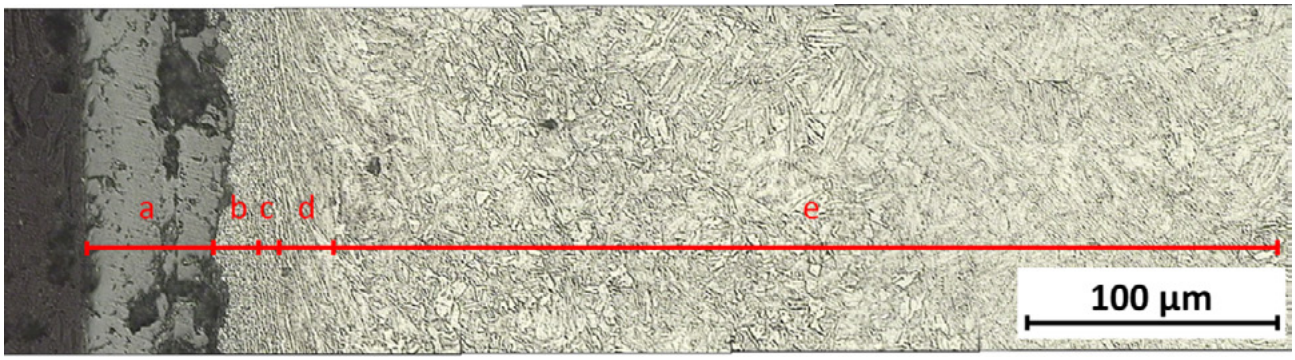

Fig. 10 – Example of an optical micrograph of the cross-section of the pins after wear tests under variable load and under the higher constant loads. The labeled areas indicate the boundary between layers. From left to right: (a) porous and spalled iron oxide layer, (b) fine and unoriented layer, (c) fine and oriented layer, (d) plastically deformed layer and (e) unaffected microstructure.

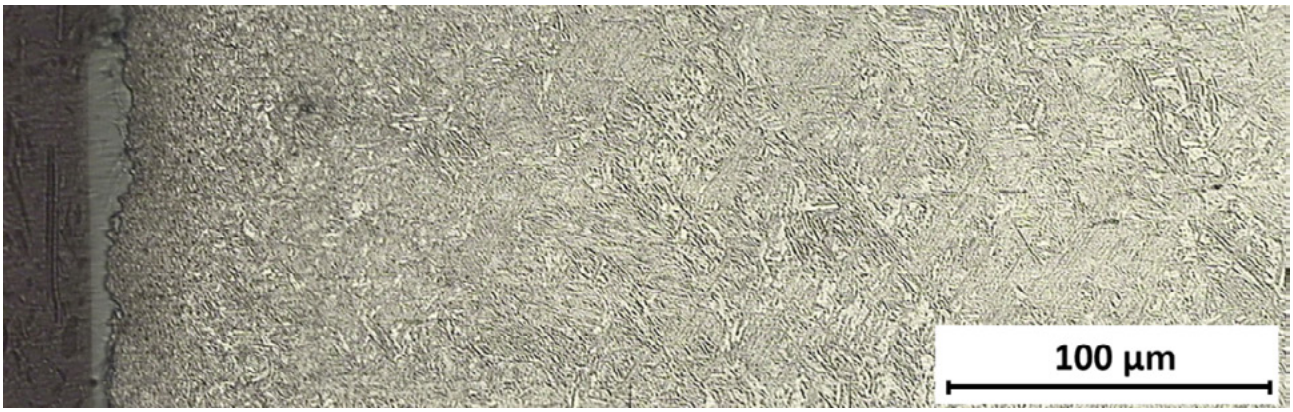

Fig. 11 – Optical micrograph of the cross-section of the pins after wear test under the constant 250 N load.

Hardness profiles of the cross-sections of pins before and after wear tests in all conditions are reported in Fig. 12. For the constant 250 and 650 N loads and the variable load, the hardness profiles follow a similar pattern. The hardness is very low at a distance of about 100 µm from the sliding interface, then progressively increases reaching a value comparable to that of the original pin. For the constant 450 N load, the hardness profile is similar to that of the original pin, but the hardness values close to the sliding interface are 200 HV0.5 lower than those recorded on the carburized layers of the original pin. Concerning the mean wear depths of pins calculated over the five tests, that under the constant 650 N load is greater than the effective thickness for the carburizing treatment and equal to 0.68 mm. Conversely, the mean wear depths of pins calculated over the five tests under variable load and the constant 450 and 250 N loads are lower than the effective thickness for the carburizing treatment and equal to 0.42, 0.28 and 0.16 mm, respectively. The hardness profile of the cross-section of pins and the mean

wear depths obtained after wear tests under the variable load and the constant 450 and 250 N loads suggest a softening of the martensitic plus carbide microstructure, associated with partial removal of the carburized layers. Under the constant 650 N load, the hardness profile and the mean wear depth of pins indicate the softening of the lower bainitic microstructure and the total removal of the carburized layer. Wear resistance is known to be negatively related to the softening of the worn surface layers [31,32]: accordingly, the softening of the material under the highest constant load is related to a worsening of wear resistance.

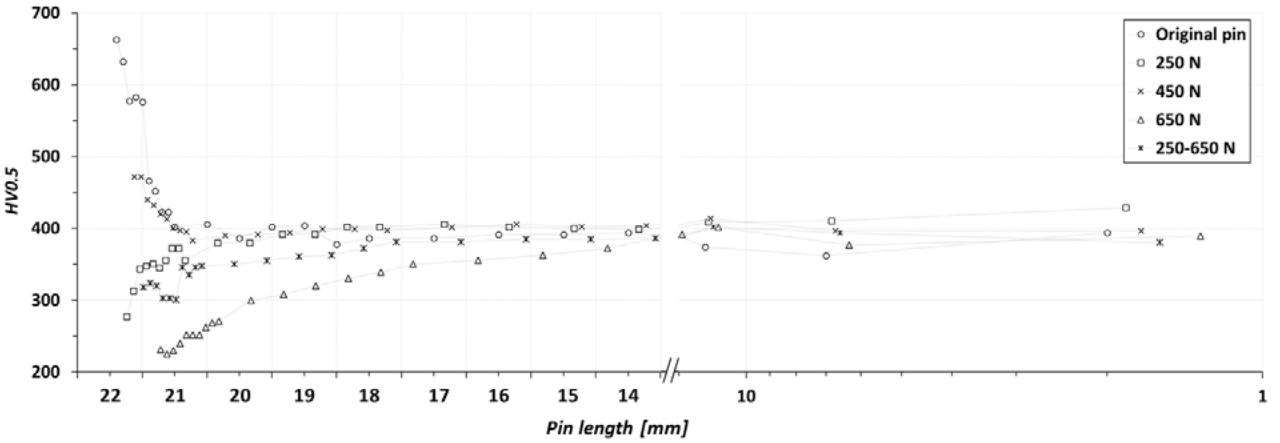

CONCLUSIONS

The effects of high constant and variable loads on a plasma-sprayed Al_2O_3-13%TiO_2 ceramic coating/steel couple are evaluated under dry sliding and in conditions similar to those occurring in heavy-duty diesel engines.

On the basis of the above-reported results, the following observations can be drawn:

• High friction and wear involve both material removal from the coating surface and oxidational wear. The sliding wear between Al_2O_3-13%TiO_2 coating and carburizing steel results in a Fe2O3 metallic film transferred onto the ceramic surface.

• The Al_2O_3-13%TiO_2 coating is under a severe-oxidational wear regime for all constant loads except at the constant 250 N load where the wear regime is between mild- and severe-oxidational. Under variable load the mean wear rate is comparable to that recorded under a constant 450 N load.

• The transition from mild- to severe-oxidational wear is associated with delamination and extensive cracking of the surface of plasma-sprayed Al_2O_3-13%TiO_2 ceramic coating, softening of the carburizing steel and removal of the carburized layer of pins.

• The usefulness of the plasma-sprayed Al_2O_3-13%TiO_2 ceramic coating/steel couple under dry sliding and in heavy-duty diesel engines may be limited to applied loads lower than 250 N.

ACKNOWLEDGMENTS

The authors would like to thank Zocca Officine Meccaniche (Funo, Bologna, Italy) for the thermally sprayed coating manufacturing, and Engineer Marco Vitali for his contribution to the experimental activity. The authors thank Prof. Fernando Guiberteau and the group GEMA in the Department of Mechanical, Energy and Materials Engineering of the Industrial Engineering School at Universidad de Extremadura for the elastic modulus measurements.

REFERENCES

[1] H.A. Bolton, J.M. Larson, Valvetrain system design and materials, in: Proc. Int. Symp. Valvetrain Syst. Des. Mater., 1997: p. 139.

[2] S. Asanabe, Applications of ceramics for tribological components, Tribol. Int. 20 (1987) 355–364. doi:https://doi.org/10.1016/0301-679X(87)90064-8.

[3] U.O. H Hazar, The effects of Al2O3 e TiO2 coating in a diesel engine on performance and emission of corn oil methyl ester, Renew. Energy. 35 (2010) 2211–2216. doi:10.1016/j.renene.2010.02.028.

[4] G. Bolelli, V. Cannillo, L. Lusvarghi, T. Manfredini, Wear behaviour of thermally sprayed ceramic oxide coatings, Wear. 261 (2006) 1298–1315. doi:10.1016/j.wear.2006.03.023.

[5] L. Fedrizzi, S. Rossi, F. Bellei, F. Deflorian, Wear-corrosion mechanism of hard chromium coatings, Wear. (2002). doi:10.1016/S0043-1648(02)00254-5.

[6] M. Laribi, A.B. Vannes, D. Treheux, Study of mechanical behavior of molybdenum coating using sliding wear and impact tests, Wear. (2007). doi:10.1016/j.wear.2007.01.018.

[7] T.A. Stolarski, S. Tobe, The effect of spraying distance on wear resistance of molybdenum coatings, Wear. 249 (2001) 1096–1102. doi:10.1016/S0043-1648(01)00842-0.

[8] F. Vargas, H. Ageorges, P. Fournier, P. Fauchais, M.E. López, Mechanical and tribological performance of Al2O3-TiO2coatings elaborated by flame and plasma spraying, Surf. Coatings Technol. (2010). doi:10.1016/j.surfcoat.2010.07.061.

[9] P.P. Psyllaki, M. Jeandin, D.I. Pantelis, Microstructure and wear mechanisms of thermal-sprayed alumina coatings, Mater. Lett. 47 (2001) 77–82. doi:10.1016/S0167-577X(00)00215-9.

[10] B. Normand, V. Fervel, C. Coddet, V. Nikitine, Tribological properties of plasma sprayed alumina-titania coatings: Role and control of the microstructure, Surf. Coatings Technol. 123 (2000) 278–287. doi:10.1016/S0257-8972(99)00532-0.

[11] M. Merlin, C. Soffritti, R. Vazquez, Effect of relative humidity and applied loads on the tribological behaviour of a steel/Cr2O3-ceramic coupling, Wear. (2013). doi:10.1016/j.wear.2013.03.043.

[12] M. Merlin, C. Soffritti, R. Vazquez, G.L. Garagnani, Effect of varying load on the tribological behaviour of a steel/Al2O3-TiO2 ceramic coating, in: 5th World Tribol. Congr. WTC 2013, 2013: pp. 1592–1595.

[13] M. Merlin, C. Soffritti, R. Vazquez, G.L. Garagnani, Friction and wear behaviour of APS and HVOF advanced ceramic coatings, Metall. Ital. 103 (2011) 17–23.

[14] C. Soffritti, M. Merlin, R. Vazquez, G.L. Garagnani, Tribological Behavior of a Cr2O3Ceramic Coating/Steel Couple Under Dry Sliding and Heavy Loading Conditions, J. Mater. Eng. Perform. (2018). doi:10.1007/s11665-018-3426-3.

[15] M. Merlin, C. Soffritti, R. Vazquez, V. Mazzanti, G.L. Garagnani, Analytical treatment of uncertainties for a macroscopic tribology instrumentation, Yejin Fenxi/Metallurgical Anal. 33 (2013) 74–80.

[16] V. Aronov, T. Mesyef, Wear in Ceramic/Ceramic and Ceramic/Metal Reciprocating Sliding Contact, J. Tribol. 108 (1986) 16–21.

[17] G.W. Stachowiak, G.B. Stachowiak, A.W. Batchelor, Metallic film transfer during metal-ceramic unlubricated sliding, Wear. (1989). doi:10.1016/0043-1648(89)90084-7.

[18] B. Wang, Z.R. Shui, A.V. Levy, Sliding Wear of Thermally Sprayed Chromia Coatings, Wear. 138 (1990) 93–110.

[19] H. Cetinel, E. Celik, M.I. Kusoglu, Tribological behavior of Cr2O3 coatings as bearing materials, J. Mater. Process. Technol. 196 (2008) 259–265. doi:10.1016/j.jmatprotec.2007.05.048.

[20] H. Goto, Y. Amamoto, Effect of varying load on wear resistance of carbon steel under unlubricated conditions, Wear. 254 (2003) 1256–1266. doi:10.1016/S0043-1648(03)00222-9.

[21] H. Goto, Y. Amamoto, C. V. Suciu, Investigations on the mechanism of quasi-mild wear for carbon steel in dry sliding contact under variable loading, and endurance of the worn surfaces, Wear. (2009). doi:10.1016/j.wear.2008.12.067.

[22] H. Goto, Y. Amamoto, Effects of a Stepwise Change in Load on the Subsequent Friction and Wear Characteristics of Carbon Steel

Under Dry Sliding, Wear. 263 (2007) 579–585.
[23] L. Lu, K. Nogita, A.K. Dahle, Combining Sr and Na additions in hypoeutectic Al-Si foundry alloys, Mater. Sci. Eng. A. 399 (2005) 244–253. doi:10.1016/j.msea.2005.03.091.
[24] D.I. Pantelis, P. Psyllaki, N. Alexopoulos, Tribological behaviour of plasma-sprayed Al2O3coatings under severe wear conditions, Wear. 237 (2000) 197–204. doi:10.1016/S0043-1648(99)00324-5.
[25] C.B. Ponton, R.D. Rawlings, Vickers indentation fracture toughness test Part 1 Review of literature and formulation of standardised indentation toughness equations, Mater. Sci. Technol. (1989). doi:10.1179/mst.1989.5.9.865.
[26] C.B. Ponton, R.D. Rawlings, Vickers indentation fracture toughness test Part 2 Application and critical evaluation of standardised indentation toughness equations, Mater. Sci. Technol. (1989). doi:10.1179/mst.1989.5.10.961.
[27] G.M. Pharr, An improved technique for determining hardness and elastic modulus using load and displacement sensing indentation experiments, J. Mater. Res. 7 (1992) 1564–1583. doi:10.1557/JMR.1992.1564.
[28] G. Straffelini, Friction and Wear—Methodologies for Design and Control, Springer, 2015.
[29] C. Monticelli, A. Balbo, F. Zucchi, Corrosion and tribocorrosion behaviour of thermally sprayed ceramic coatings on steel, Surf. Coatings Technol. (2011). doi:10.1016/j.surfcoat.2011.01.023.
[30] F.H. Stott, The role of oxidation in the wear of alloys, in: Tribol. Int., 1998. doi:10.1016/S0301-679X(98)00008-5.
[31] Y. Wang, T. Lei, J. Liu, Tribo-metallographic behavior of high carbon steels in dry sliding I. Wear mechanisms and their transition, Wear. 231 (1999) 1–11. doi:10.1016/S0043-1648(99)00115-5.
[32] Y. Wang, T. Lei, J. Liu, Tribo-metallographic behavior of high carbon steels in dry sliding III. Dynamic microstructural changes and wear, Wear. (1999). doi:10.1016/S0043-1648(99)00117-9.
[33] E. Takeuchi, Friction and wear of machine parts -surface heat treatments for increase wear resistance, Mach. Tools. 23 (1979) 68–74.
[34] Y. Wang, T. Lei, J. Liu, Tribo-metallographic behavior of high carbon steels in dry sliding II. Microstructure and wear, Wear. 231 (1999) 12–19. doi:10.1016/S0043-1648(99)00116-7.
[35] S.M. Hsu, M. Shen, Wear prediction of ceramics, Wear. 256 (2004) 867–878. doi:10.1016/j.wear.2003.11.002.
[36] K. Kato, K. Adachi, Wear of advanced ceramics, Wear. 253 (2002) 1097–1104. doi:10.1016/S0043-1648(02)00240-5.
[37] H.S. Ahn, O.K. Kwon, Wear behaviour of plasma-sprayed partially stabilized zirconia on a steel substrate, Wear. 225–229 (1993) 814–824. doi:10.1016/0043-1648(93)90556-2.